Chapter 13: Using Energy Envelope to recognize cratering

Copyrighted by WR. Barnhart, 5/1/2021

Abstract

The concept of an energy signature is used to recognize previously unidentified cratering systems on the moon and earth. Recognizing the Fermi-Pavlov and Pirquet-Ramsay Basins on our moon illustrates the method. Solving the origin of grooves on Phobos, Mars's larger moon, as CGRS from known and ghost craters demonstrates the validity of the concept. Finding craters, from their energy signature, at the sight of the Tunguska, Siberia, air burst, provides a cratering source for the Planar Deformation Features found in samples there.

The F-Pv Basin

Moscovience and Freundlich-Sharonov Basins were consider in Chapter 12 on the far-side of the moon. They both exhibit the same red center (a mascon of high gravity) in GRAIL maps, a blue rings of very low gravity surrounded by a red ring of high gravity, then a second blue ring, and second red ring (Figure 12.12-15). While these are referred to as "basins", they are both certainly individual large impact craters. Their alternating low and high gravity reading, often with their corresponding high and low topography, with a sudden change in between indicating the site of the adiabatic transition, is referred to as the energy signature.

In the southwest quadrant of our moon's farside, centered at latitude -21.6615^{o}N and longitude 132.6042^{o}E and latitude -31.4799^{o}N and longitude 141.1322^{o}E are two other cratering basins that have not been previously recognized, Figure 13.1. I will refer to them as the Fermi-Pavlov Basin (F-Pv) basin (~750 km diameter) and the Pirquet-Ramsay Basin (P-R) (~660 km diameter) respectively. That these are not the only ghost craters that can be identified in this area is shown by Figure 13.2.

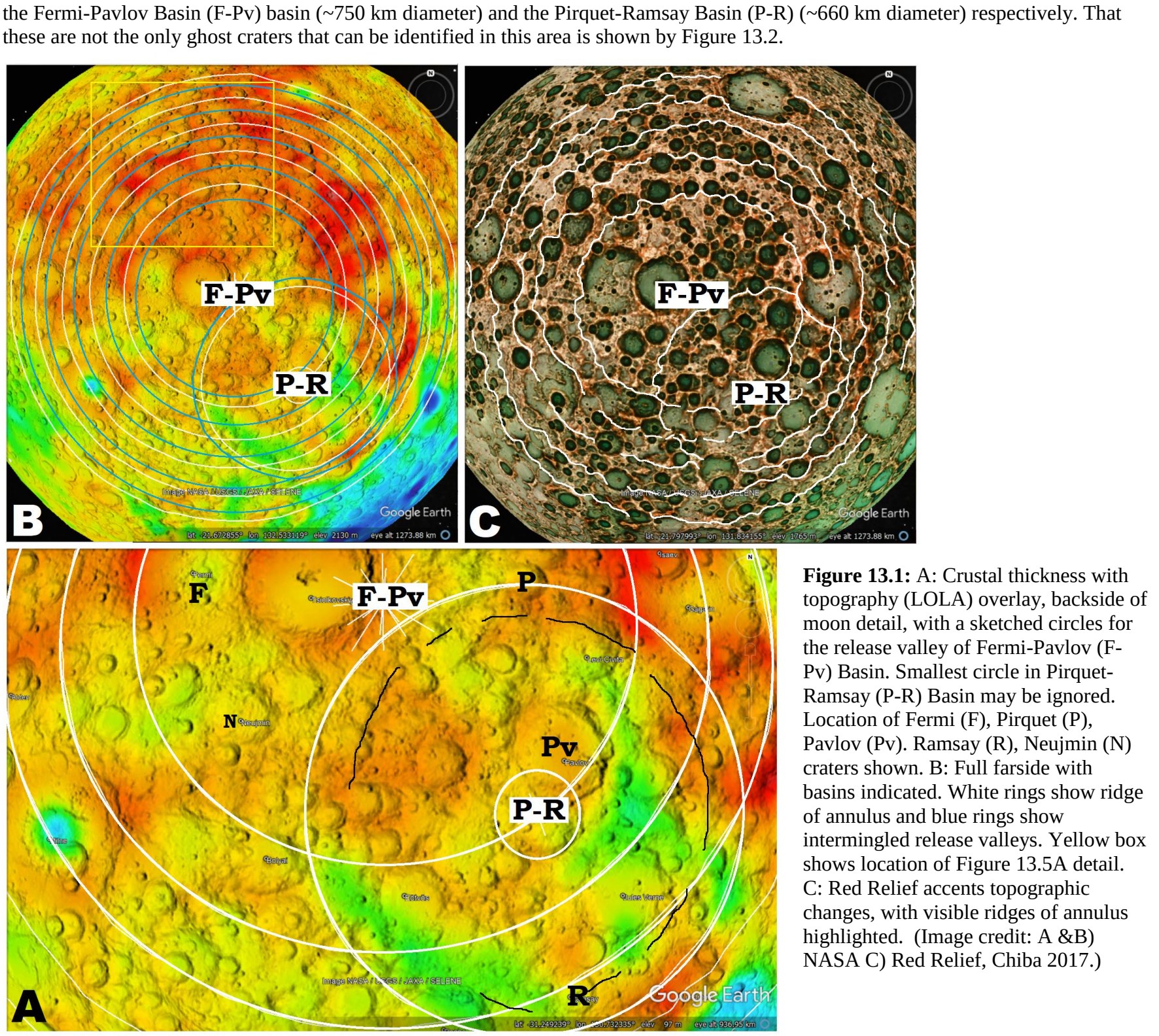

Figure 13.1: A: Crustal thickness with topography (LOLA) overlay, backside of moon detail, with a sketched circles for the release valley of Fermi-Pavlov (F-Pv) Basin. Smallest circle in Pirquet-Ramsay (P-R) Basin may be ignored. Location of Fermi (F), Pirquet (P), Pavlov (Pv). Ramsay (R), Neujmin (N) craters shown. B: Full farside with basins indicated. White rings show ridge of annulus and blue rings show intermingled release valleys. Yellow box shows location of Figure 13.5A detail. C: Red Relief accents topographic changes, with visible ridges of annulus highlighted. (Image credit: A &B) NASA C) Red Relief, Chiba 2017.)

Figure 13.2: Sketch of some of the less distinct circular (red circles) and straight linears (blue arcs) visible in the vicinity of F-Pv and P-R basins. The occurrence of ghost craters and CGRS fill the area. (Image credit: Google Earth with NASA overlay.)

An even larger rings, the Gagarin-Hopmann (G-H) basin is obvious in GRAIL data (Figure 13.3A) by its nearly complete ring of red, high density surrounding blue and green of lower density in the southern half of the moon's farside. While it is quite visible in GRAIL density, it is nearly invisible in Crustal Thickness except for its center (Figure 13.3B). If a ~1000 km diameter crater can be totally hidden on the farside while Maria of similar size are obvious on the front-side, it implies significantly different cratering process on the two sides. This will be explored in later chapters. If it ever had a mascon in its center, it is totally masked by rims from later cratering. This holds a significant example for mountainous areas on the earth, like the Rocky Mountains.

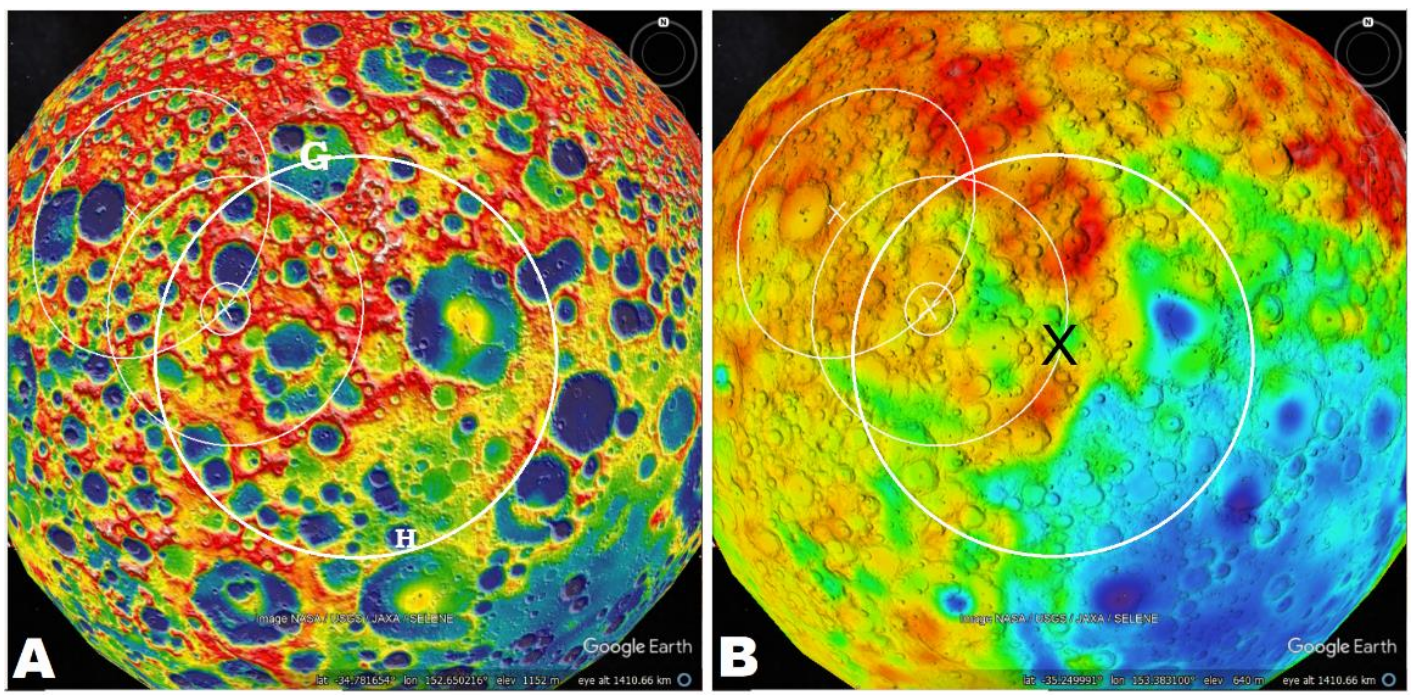

Figure 13.3: Gagarin-Hopmann (G-H) basin, southwest quadrant farside of the moon. (A) GRAIL overlay to Google Earth, Moon, with F-Pv and P-R basins shown for comparison. (B) Crustal Thickness with LOLA data overlay to Google Earth, showing with an "x" the approximate location of center: Latitude -35.655^{o}N, longitude 154.406^{o}E. (Image credit: Google Earth with NASA overlays.)

The F-Pv and P-R basins became recognized while I was looking at the interaction of the Fermi and Tsiolkovskiy craters for another topic. The F-Pv and P-R basins were first visible as the intersection of two round circles on the crustal thickness map. They are highly affected by the under-print of the South Pole-Aitkin crater, southeast blue area in Figure 13.3).While neither of them show the classic bowl shape of crustal thickness like Marie Orientale, Nectaris, or Moscoviense (Figures 11.1, 11.4, and 11.8 respectively), they do show some thickening of the crust under the smallest white ring which I will designate the OCR ring. This thickening is most prominent on the northern half of the F-Pv basin (Figure 13.1B) and three separated sections, west, northeast and southeast of the P-R basin. Much of the southern edge (Figure 13.1A) between Neujmin Crater (N) to Pavlov crater shows correlation with red, thicker crust, if less distinctly thicker. While the thinned crust is expected within the designated OCR of these craters is only indicated by the green area in the P-R Basin, it lies more along two lines than the arc of a circle. These linears correspond with the energy signature of several CGRS, Figure 13.2.

This type of obscuring of both the high and low gravity areas is connected with extensive later cratering, Figure 10.6, 8, and 10 where it is attributed to the energy envelope of later impactors being lost in the heat of the substrate produced by earlier impactors. In this case it was the South Pole-Aitken Crater/Basin. This indicates cratering took place so rapidly that it did not allow heat to dissipate significantly before more impactors arrived.

While occurrence of the rings in Figure 13.4, within the energy signature, is not continuous, they can be recognized as multiple points indicated by the blue arrows. Multiple layers of craters, each adding their individual energy signatures into a molten or highly plastic substrate form complex overlapping ripple patterns just like ripple patterns in a puddle of water (Figure 10.1-5). These original ripple patterns may require hunting for, but they do often still exist.

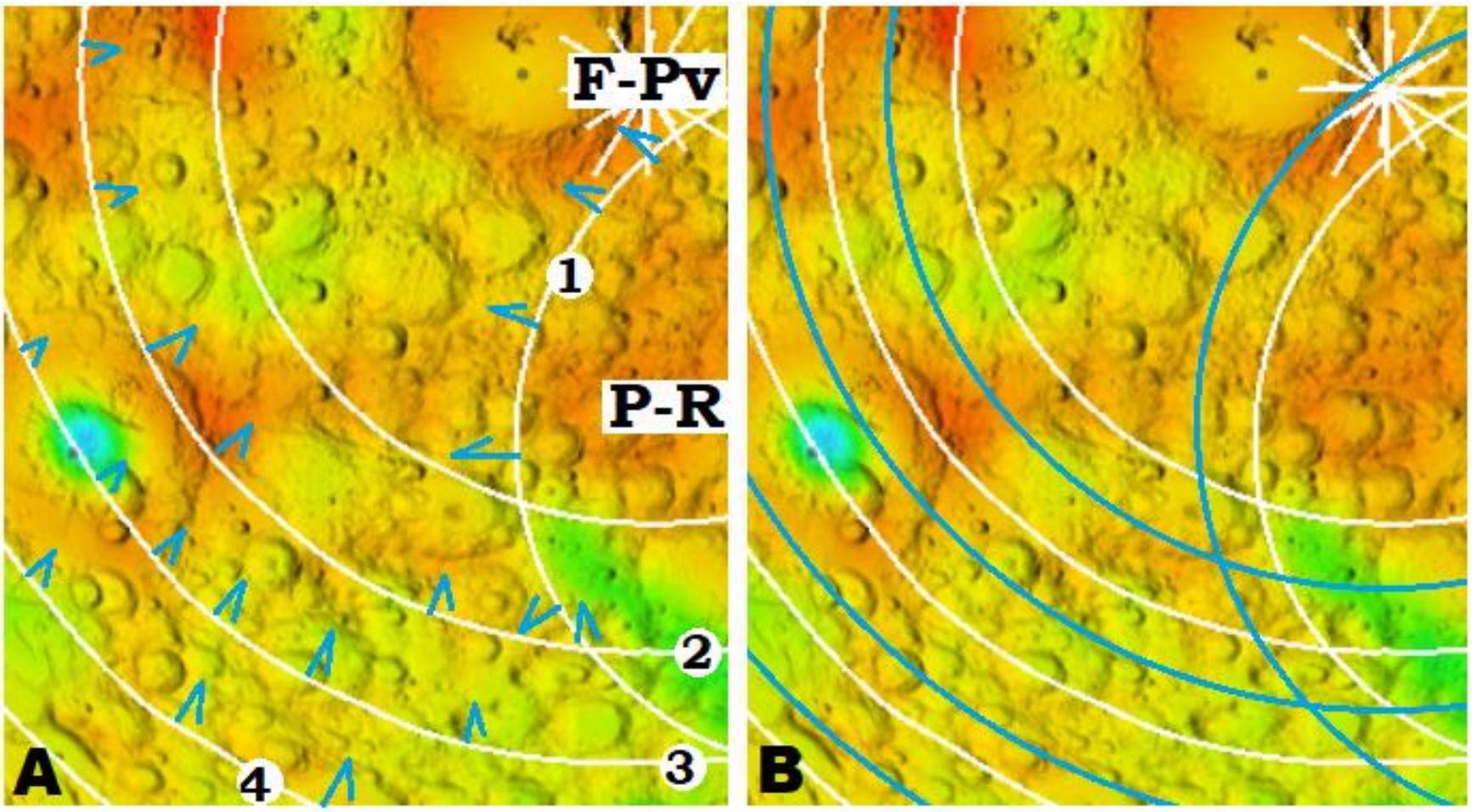

Figure 13.4: A: Arrows point to release valley low. B: White circles generally follows gravity high and blue circles follow gravity lows. (Image credit: extracted from west half of Figure 13.1A.)

Figure 13.5 shows extending the concept of finding the release valley linear to the northern half of the F-PV basin. Even when craters occur centered between the two shock wave ridges, their upthrust ridge is lower, showing they had to override the low energy signature of the release valley they impacted within. Because the adiabatic envelope has to burst to allow this move, the shock wave ridge combined with the release valley low accounts for the total energy signature of a crater. We are not seeing one impact crater covering another or obliterating the first. Instead, we see the final cratering pattern as the cumulative energy for each spot during the full time of the cratering process, where each new impact adds to the total energy pattern already there.

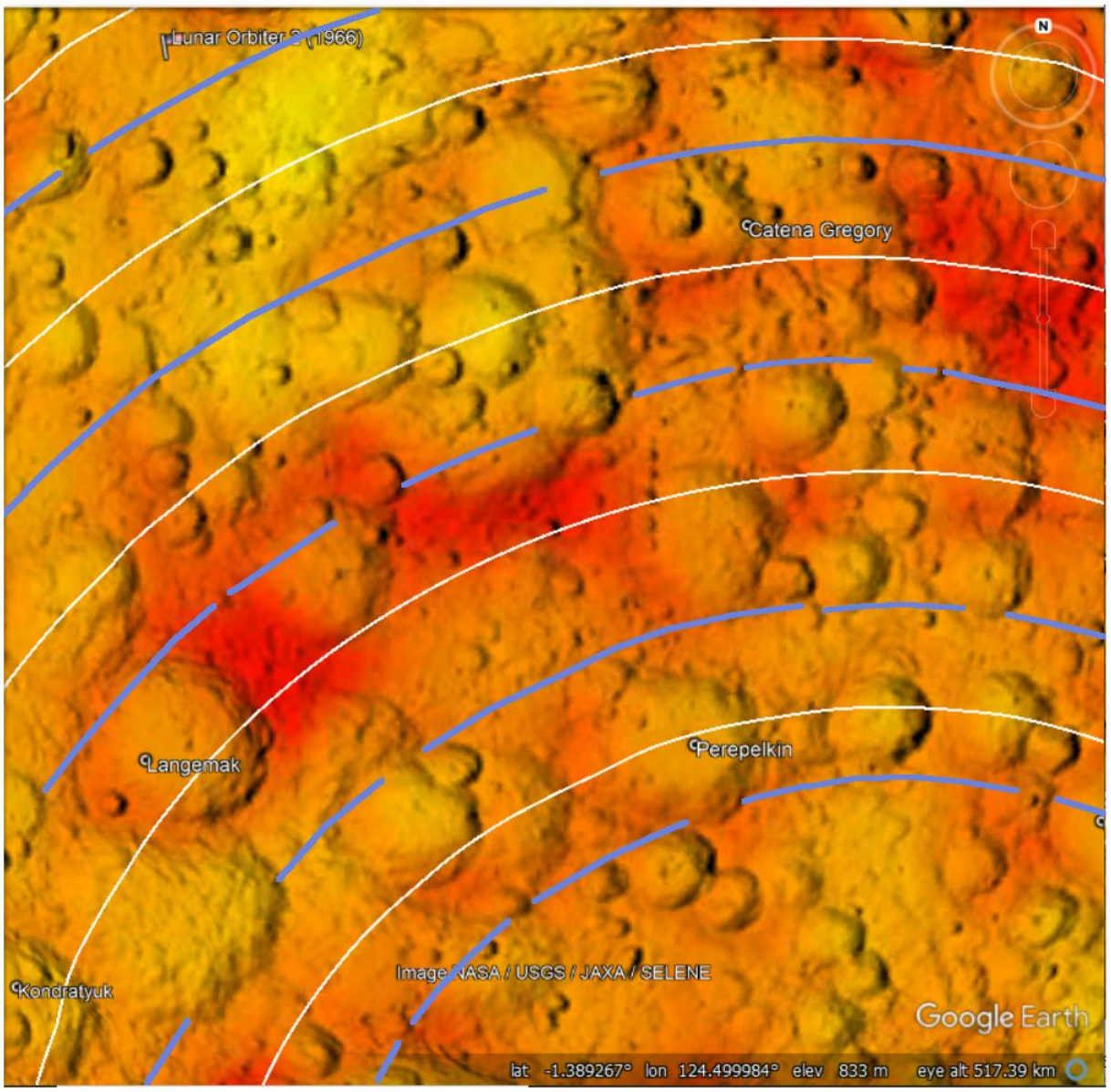

Figure 13.5: F-Pv basin showing the linears from the release valley in the LOLA data blended with crustal thickness. White arcs showing high topography, and blue arcs showing low gravity/release valleys. (Image credit: detail from Figure 13.1B.)

Phobos, Mars's battered moon

Not a sphere but "potato" shaped, Phobos is the larger moon of Mars and has dimensions of 28.8 x 22.4 x 18.4 km/17.9 x 13.9 x 11.4 miles (NASA 2013). Very small by the standard of Earth's moon, it is also in a much closer orbit. Its most obvious feature (Figure 13.6) beyond the large crater, Strickney (9 km/5.6 miles), is its grooves. The "grooves" are filled with irregularly pitting or small craters (Figure 13.7).

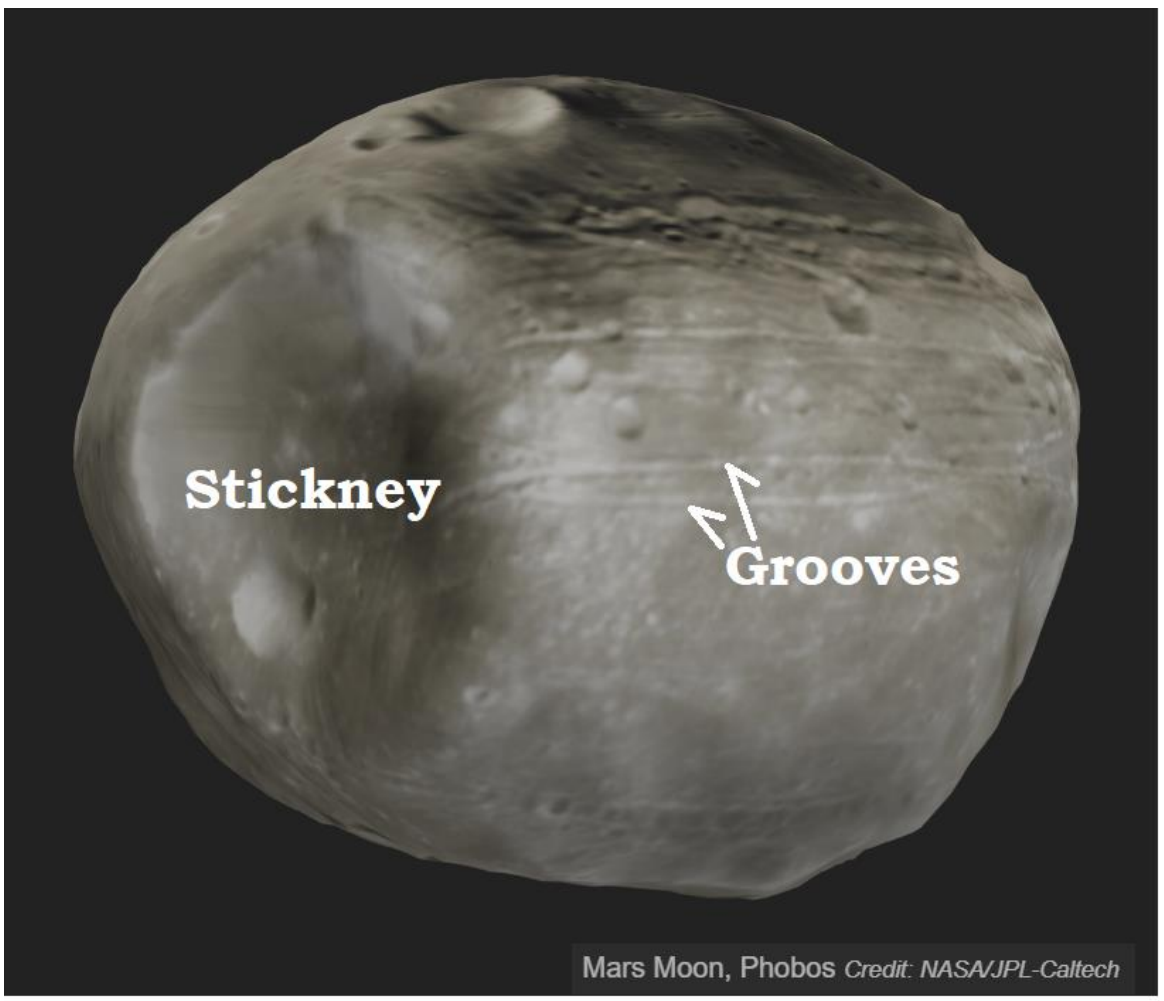

Figure 13.6: Phobos as seen from Mars's surface. With Stickney on its western edge. (Image credit: Viking Project, JPL, NASA: E.V. Bell II (NSSDC/Raytheon ITSS)

Three possible sources of Phobos are recognized, that it accreted at the same time as Mars (Ronnet et al. 2016), that it was captured – but Ronnet et al. recognizes it low eccentricity and prograde orbit rules out capture, – or that it was the byproduct of a large impact on Mars's surface (Hyodo et al. 2017a, Hyodo et al 2017b).

As for the origin of the Phobo's grooves, several theories attempt to account for them. Some of the first suggested they were a result of tidal stresses created between Mars and the locked position of Phobos (Soter and Harris. 1977), or they are chains of secondary impact craters formed by ejecta from primary impacts craters on Mars's surface (Murry and Iliffe 2011), or maybe rolling and bouncing trails from rocks directly ejected by Stickney crater (Wilson and Head 2015).

Two mechanisms for the grooves are favored at present, and it is thought that together they account for all of the grooves. First, grooves that are approximately in the plane parallel to Mars's surface were produced by tidal forces due to orbital decay, and are the first sign that Phobos is slowly pulling apart (Hurford et al 2016). The grooves that are approximately perpendicular to these were produced by returning ejecta from the Strickney cratering event, traveling at a lower velocity and rolling and bouncing in circles or spirals around the potato shape (Nayak and Asphaug 2016).

Whether Borealis Basin is the source of the material for Phobos as Hyodo et al suggest, or if Mars experienced an impact history nearly as extensive as I am suggesting for the Earth, there most likely was extensive splatter into orbital space. In the coalescing of Phobos (Pignatale et al. 2018) from gases and solids, addition accretion would also include much splatter in the molten form at 1800^{o}C (Hyodo et al 2017a). By gathering the splatter up quickly enough, the resultant composition would be an ultramafic magma. Subsequent collisions with large blobs of splatter or additional impactors would produce the shock heating and adiabatic cooling for producing the dominance of phyllosilicate, particularly around Stickney crater, where this subsequent impact is obvious. The general spectral results suggest there was a full ultramafic assemblages including some Felspars/Felspathoids (Gieranna et al 2010).

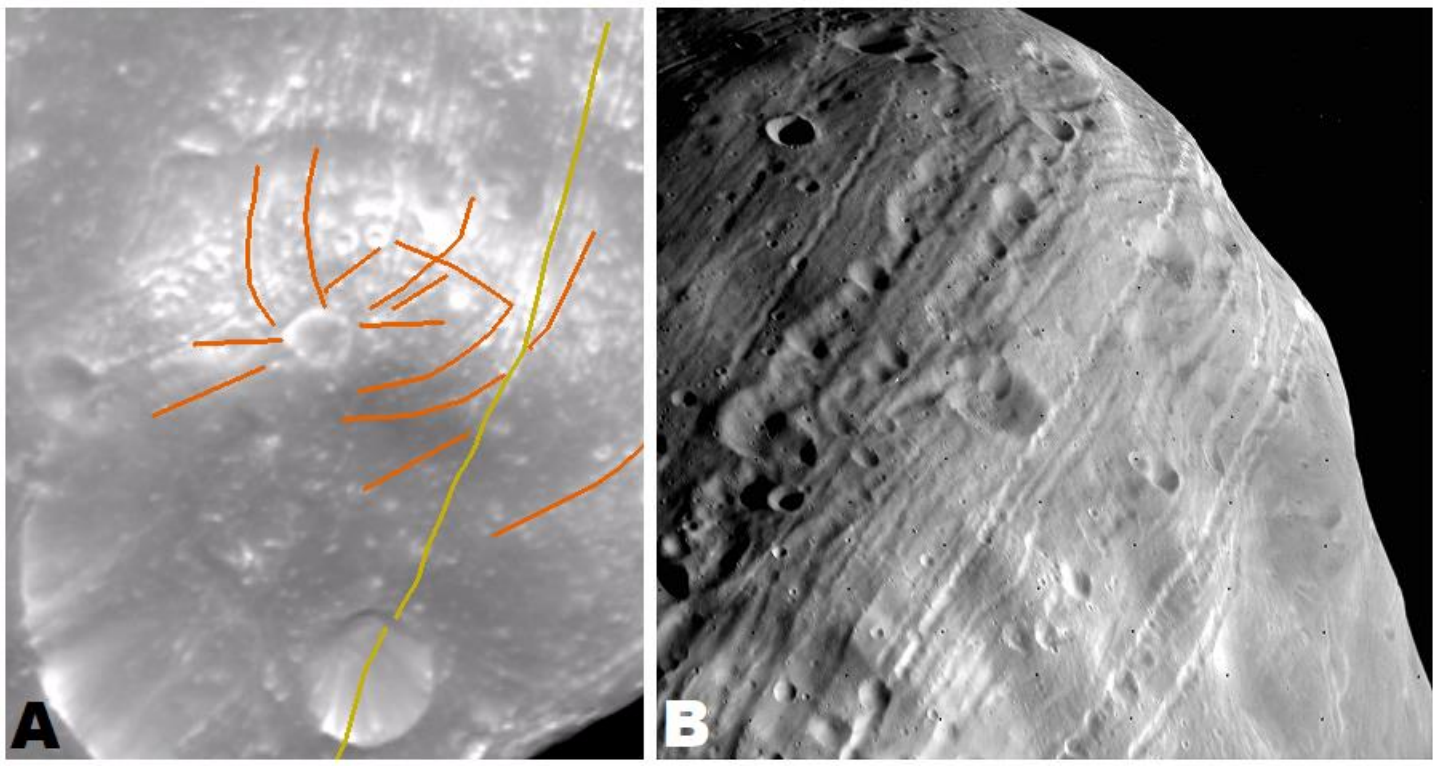

Figure 13.7: Different conditions of lighting, angles, and resolutions make visibility of the grooves very different. A) Strickney crater with Limtoc crater near the bottom. Large light spot across the top is vicinity of crater 5, Figure 13.8. B) Central third of the light area of "A" with Strickney crater just off to lower left. Irregular pitting or small craters are seen to form many groves. (Image Credit; A) detail of ESA Mars Express 17 November 2019. B) Viking 1 Orbiter, NASA.)

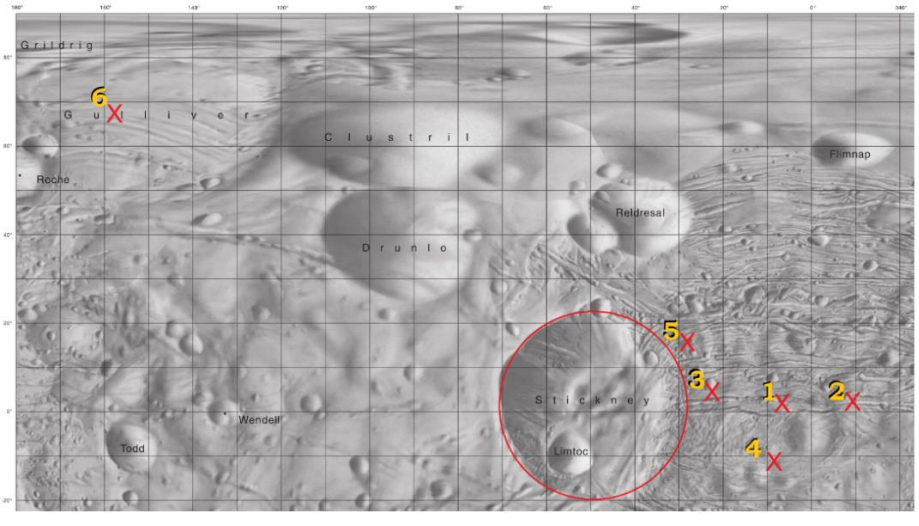

The mystery of Phobos grooves

The gathering-up of splatter followed by subsequent collisions or impactors would produce extended annulus or CGRS to those collisions, and the grooves are evidence of those CGRS. Figure 13.8 shows the location of the six craters discussed here.

Figure 13.8: A portion of the northwest quadrant of the cylindrical-grid projection, labeled map of Phobos, showing the location of the six craters discussed. (Image Credit: U.S. Geological Survey – http://planetarynames.wr.usds.gov/images/phobos-cylindrical-grid.pdf./ P. Stooke, accessed 7/15/2020.)

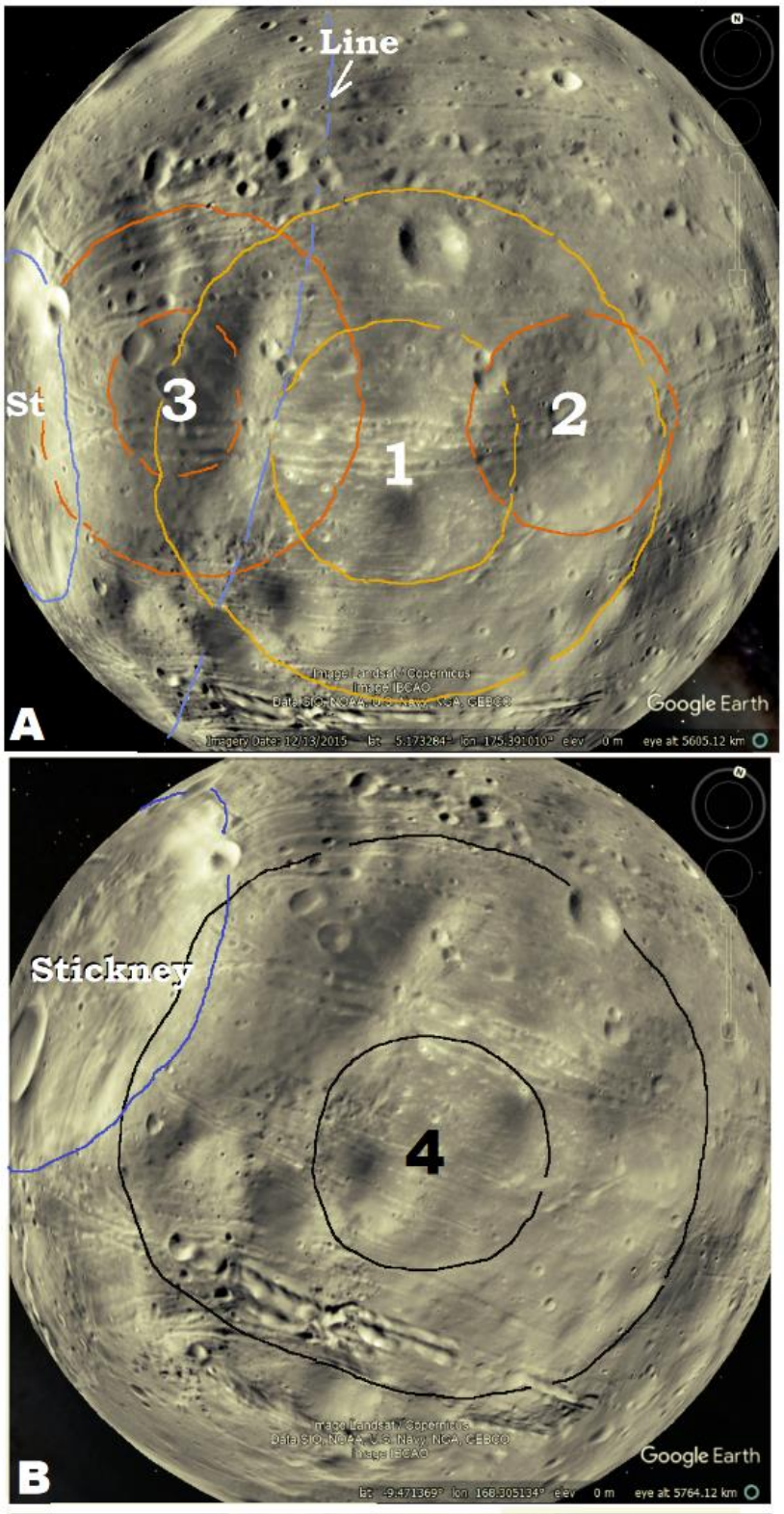

Wrapping an equal area projection of the “potato” shaped Phobos around a sphere, like Google Earth, is fraught with problems, but it allowed the use of higher resolution data than was available for Figure 13.6, and allowed circular shapes to be seen and tumbled in relative 3D over the complete surface of the moon. Figure 13.9 provides three typical views. I am postulating the impacts took place while Phobos was in a highly plastic/liquid state, so most circles will show up as ghost craters, where the shock energy signature was only minimally evident above the background energy pattern of the body.

Circle 1 (Figure 13.9A) is evident with the greater visibility of the grooves across the center of a crater, as also demonstrated in the Free Air Gravity image of Mare Orientale (Figure 11.1), As these lines in Mare Orientale are low gravity, it suggest the grooves are also low gravity, release valley, linears. A high density ring exist under the smaller yellow ring. Whether it is an Open Ring or the OCR is impossible to determine, but a distinct second high density ring also exist under the second yellow ring. That the area between the two yellow rings is a low density ring is consistent with the visibility of circle 2 and the circular linear produced by the overlap of circle 3. The circular shape of crater 2 is obvious when viewed centering on it and the prominence is consistent with the prominence of the blue low gravity crater centers seen in the low gravity (blue) rings around Moscoviense Basin (Figure 11.8B). The blue line (Figure 13.9A) that cuts off the low gravity expression of circle 3 is the expression of the shock wave portion of a CGRS. The smaller circle of 3 is visible when viewed center on it.

Circle 4 (Figure 13.9B) is drawn on a second projection so it could be centered and to provide less confusion with overlapping circles from circle 1. The circular pattern of 4 is most clearly seen on both rings as the shock-release energy signature patterns in the grooves. The release valley inside the second ring is obvious by the gaps in the lower set of grooves that cross it.

Figure 13.9: Three views of Phobos equal area map stretched over the globe of Google Earth. (Image credit: Global map Viking Orbiter, Planetary Data Systems/P. Stooke laid over Google Earth.)

The smaller circle of 5 (Figure 13.9C) at first appears much smaller and shifted to the north until the view is centered on it, and the depressed ellipse on the east side can be seen to extend to the full half circle. Again, both rings are most highly visible where the shock wave’s compression had the most effect on the release pattern in the grooves.

Figure 13.10 emphasis the ghost quality of these 5 craters, as none of them can plainly be seen on the general image of Phobos. These circles are all transferred by their relationship to recognizable landmarks.

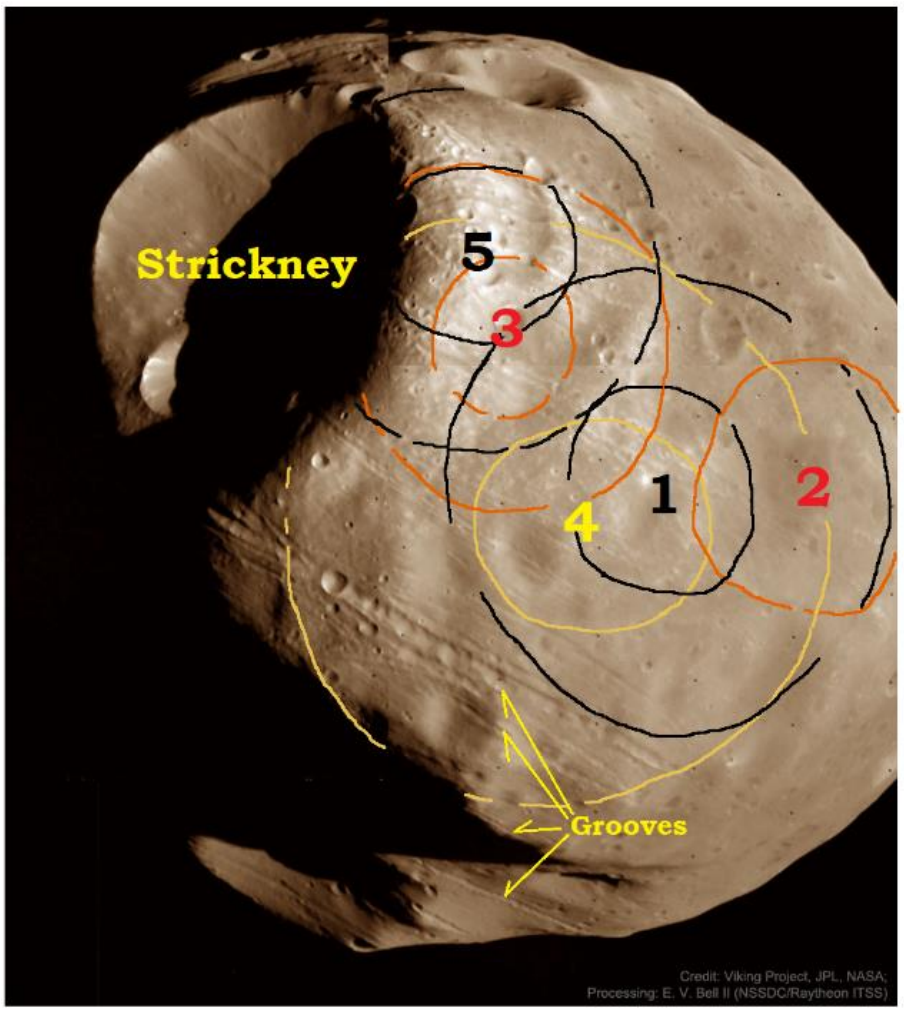

Figure 13.10: Phobos with the locations of ghost craters 1-5 indicated on its surface. (Image credit: Viking Project, JPL, NASA; E.V. Bell II, NSSDC/Raytheon ITSS)

When the surface of the earth's moon is surveyed closely for indications of impact of every size, as in Figures 9.6 and 9.8, 9.10, 10.3, 10.7-10, the number and size of the craters indicate that it was nearly saturation for each size. The craters we see are more a matter of preservation than density or pattern of impact. Considering a whole rocky body, it is reasonable to expect a random pattern of impacts and it is as likely for impacts to strike at one spot as another. If we have 100 impactors striking in a square kilometer, it is likely that approximately 100 impactors struck in every square kilometer. Thus, a limited line of craters is more likely to be a phenomena of preservation rather than an impact pattern. As with the occurrence of ghost craters on our moon, if the body of Phobos was highly viscous liquid or very plastic and of high temperature when the impacts struck, their individual energy signature would become lost in the already present heat signature. This would especially be true of the areas of highest temperature where the shock/compression wave was expressing (crater rim). This would not be less true of the low density, low temperature areas, specifically in the release wave valleys, so craters would preferentially show up there. This is what we find in linears of cratering pits within the grooves.

Comparing the grooves on Phobos to similar structures, lines of craters, on our moon (Figures 13.2 and 13.11), lines are most visible when the low density of the crater center occurs in the low gravity, release valley portion of the CGRS. This can be seen in many places on earth's moon in GRAIL. Figure 13.11 shows linears of blue and green leaving Mare Moscoviense and between Hertzsprung crater and Mare Orientale

An important point, the basic pattern of a crater is round, because the shock-release wave acts always at equal distance, so also a CGRS will often appear as a straight line because it is the result of the shock-release wave acting in a small circle intersection with the sphere of the earth, moon or other object, which show up as a slightly arcuate or straight line, Figure 1.3B. The energy of the CGRS was already in the substrate when the pits were formed. Partial pits are just as clear as full pits. Had the pits a common origin no partial pits would be seen, as around Fermi-Tsiolkovskiy craters, Figure 2.9.

When the center of circle 1 is used to draw a series of concentric circles with Google Earth, using the program supplied to me by Marten 't Hart, it is apparent that several groups of the grooves lie concentric to that shear center (Figure 13.12)

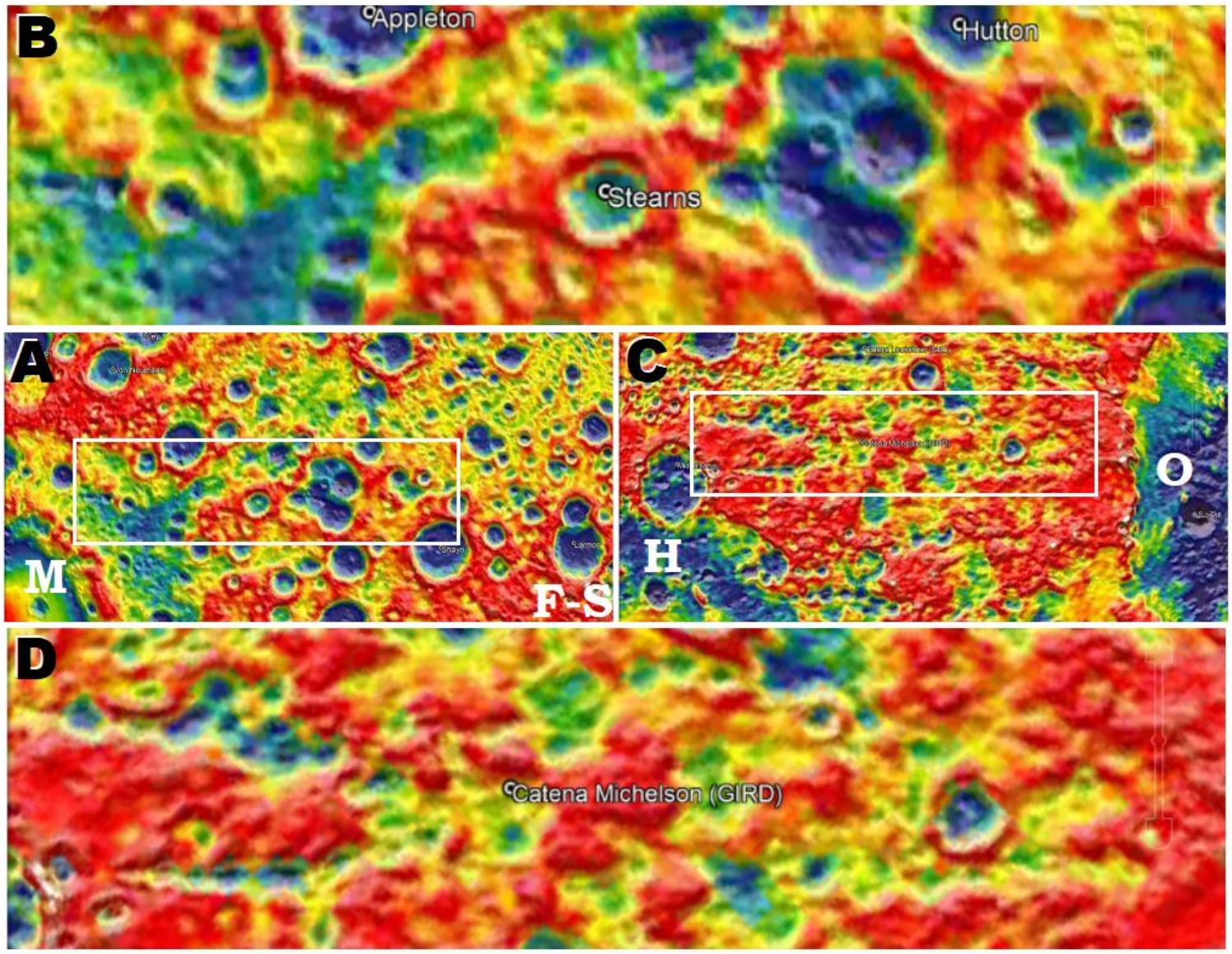

Figure 13.11: Blue lines of low gravity craters on the Luna surface. A) Northeast of Mare Moscoviense (M), north of Freundlich-Sharonov (F-S) Basin (Figure 12.12), B) Detail from A. C) Between Hertzsprung (H) crater and Mare Orientale (O). (Image credit: GRAIL overlaid on Google Earth, Moon. NASA/USGS/JAXA/SELENE.)

Figure 13.12: Red lines indicate grooves concentric to circle 1 and CGRS from that impacts. Blue lines indicate grooves visibly cut by the circle/ring of 1. (Image credit: Equal Area map overlaid to Google Earth. Google Earth data is not relevant.)

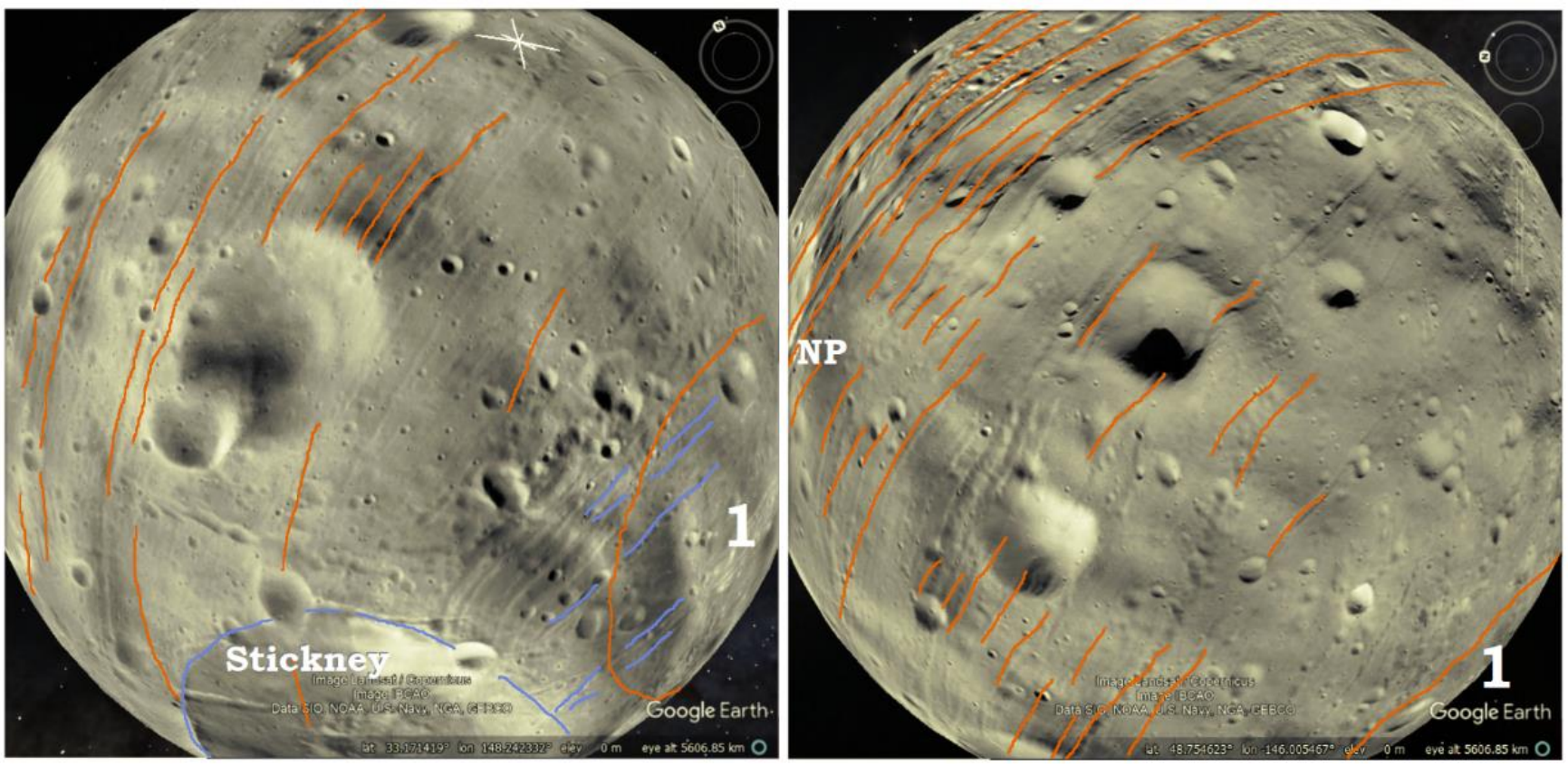

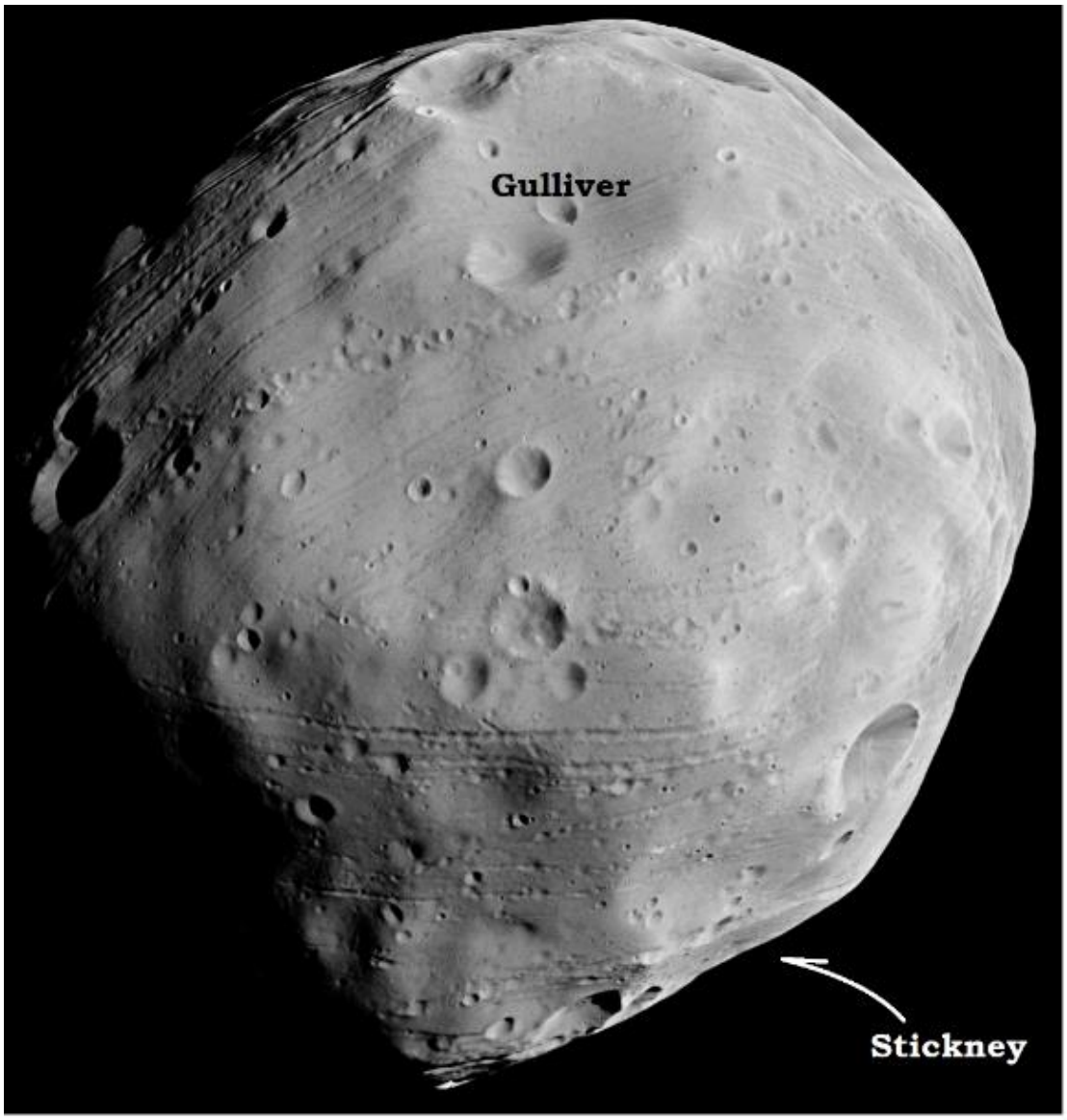

The location of circle 6 corresponds with Gulliver Crater (Figure 13.8). Figure 13.13 gives the location of Gulliver crater near Phobos's north pole and on the backside from Stickney. Figure 13.14 shows where grooves concentric to Gulliver Crater are most visible on Phobo's backside. "A" is located west of "B".

Figure 13.13: The location of Gulliver Crater just south of the north pole of Phobos (the geographic north pole is just to the west of the apex in this image), and its relationship to Stickney. (Image credit: ESA/DLR'FU Berlin (G. Neukum)/E. Lakdawalla)

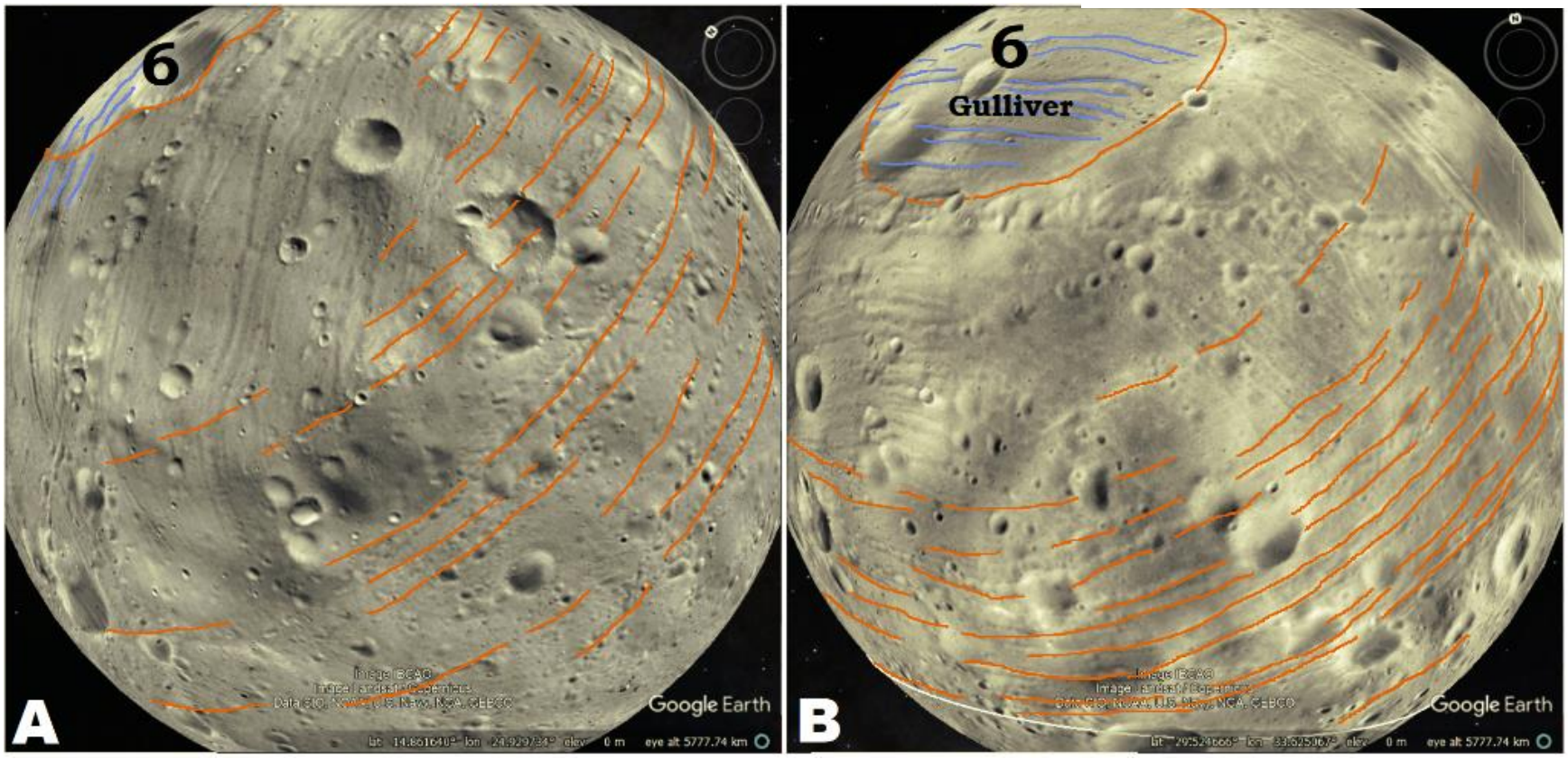

Figure 13.14: Red linears are concentric grooves to Gulliver Crater as determined by concentric circles to center of circle 6. Blue lines, grooves in Gulliver Crater, the interruption of which defines circle 6. (Image credit: Equal Area map overlaid to Google Earth. Google Earth data is not relevant.)

Yet, the prominent groove across Stickney Crater that also intersects smaller Limtec Crater (Figures 13.15 and 13.7A) may be more prominent because Gulliver Crater may have formed after Stickney Crater, but the multitude of other grooves suggest their energy

signatures were already in the substrate when Strickney formed. This emphasizes crater formation is not a ballistic ejection, but an energy event as determined in Chapter 8.

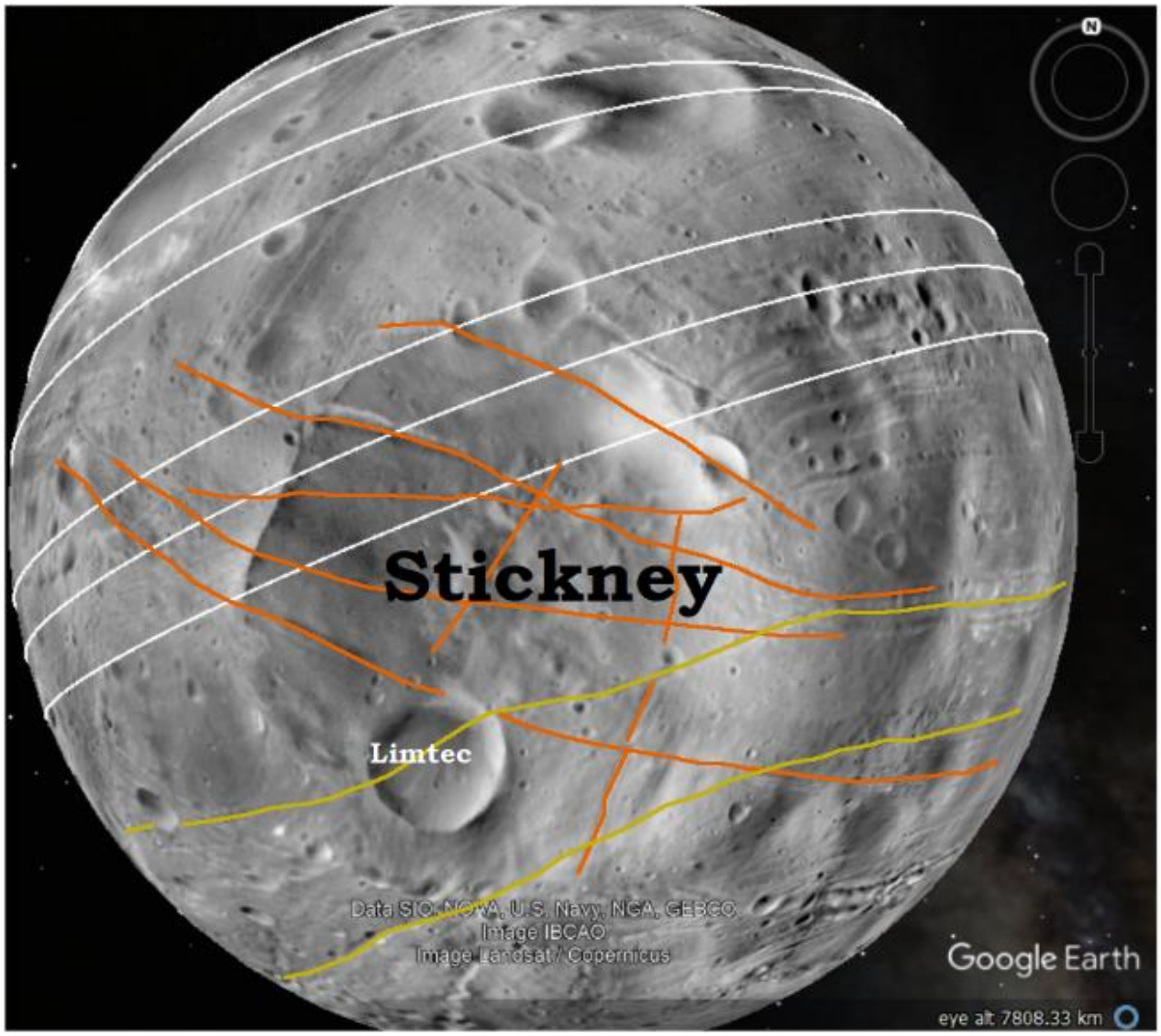

Figure 13.15: Concentric circles to circle 6 with grooves crossing Stickney Crater. It is not likely that grooves postdate Stickney's formation. Yellow linears, CGRS to Gulliver Crater. (Image credit: Equal Area map overlaid to Google Earth. Google Earth data is not relevant.)

Phobos Conclusion

If Phobos accreted from orbiting splatter ejecta in a molten or plastic state, it holds interesting alternatives for such splatter from an earth's impact episode. If the association of phyllosilicate and Felspars/Felspathoids can be associated with impacts on Phobos, we need to look harder at the abundant occurrence on our planet and recognize their association with shock heating and adiabatic cooling on earth.

Tunguska, Siberia

In Chapter 12, when discussing indicators of impact, it was mentioned that two researchers (Vannuchi et al 2015 and Hryanina, L.P., 1999.) found PDF in the area of the Tunguska bolide's midair explosion, but failed to identify any impact craters. Part of the problem in not recognizing the many craters that could be recognized if the energy signature of shock-release wave pattern is used. When we do not do so, we are ignoring much of the evidence sitting at our finger tips.

Observing the area in a terrane map prepared by Vannuchi et al, Figure 13.16. The area he gives includes at least four CGRS, Figure 13.16A. I have represented each with both a red line on the high and the blue line somewhere in the release valley towards the next ridge. Then, 1a, 2a, 3a, and 4a represent the thrust of the shock wave, Figure 12.17I, and the hollow of low gravity/valley, extends at least to the blue, "b" lines. This results in a distinct low gravity valley where CGRS 1, 2 and 3 cross and the adiabatic expansion/release wave material was immediately washed out of the valley. CGRS 4 encloses a second slightly meandering valley. This provides evidence of slower draining water erosion after the release valley formed, rather than a rushing wave of water, totally clearing the valley would produce.

Now looking at the perimeter of the central area, a distinct ring is seen in the mountain peaks. At first it looks like a single circle would account for all of these peaks, but when a perfect circle is drawn, Figure 13.16B, while many points match up to the compass circle, nearly all of the way around except for the actual valley, where the low from the CGRS is swallows up the energy thrust for the rim. A little bit of study and a second circle is recognized in the missed mountain peaks. It is not a matter of forcing them to fit, but recognizing that a second circle fits these peaks, Figure 13.16C, with nearly as many points corresponding as circle one. That the centers of both circles lay in the center of a release valley is not unexpected. Many smaller blue crater centers, round low gravity centers, can be recognized within the blue ring, low gravity ring, of a larger crater. It is not that the impactors struck there preferentially, but the preservation was preferential, like with Phobo's pitted grooves. Looking back at Figure 13.3A, five crater's dark blue interior show prominently in the southwest edge of the G-H basin, and the line of craters is extended by at least four more outside the rim of the basin. Not only do the five craters lie within the OCR from the G-H basin, which would be dark blue/low gravity of its own accord, but they lie in a line with the other dark blue craters, in a distinct gravity pattern from the CGRS they overlap.

Eventually, six overlapping craters account for most of the peaks, and they all center on this same valley. When Vannuchi et al and Hryanina (1999) try to discern the origin of their Planar Deformation Fractures they need to consider these ghost craters as likely sources.

Because Planar Deformation Fractures involves the shock wave fracturing rigid material, it might not display in a less than rigid substrate. In true ghost craters, where the energy signature becomes largely lost in the already present heat pattern, very likely the substrate is plastic enough that it would absorb the shock without fracturing.

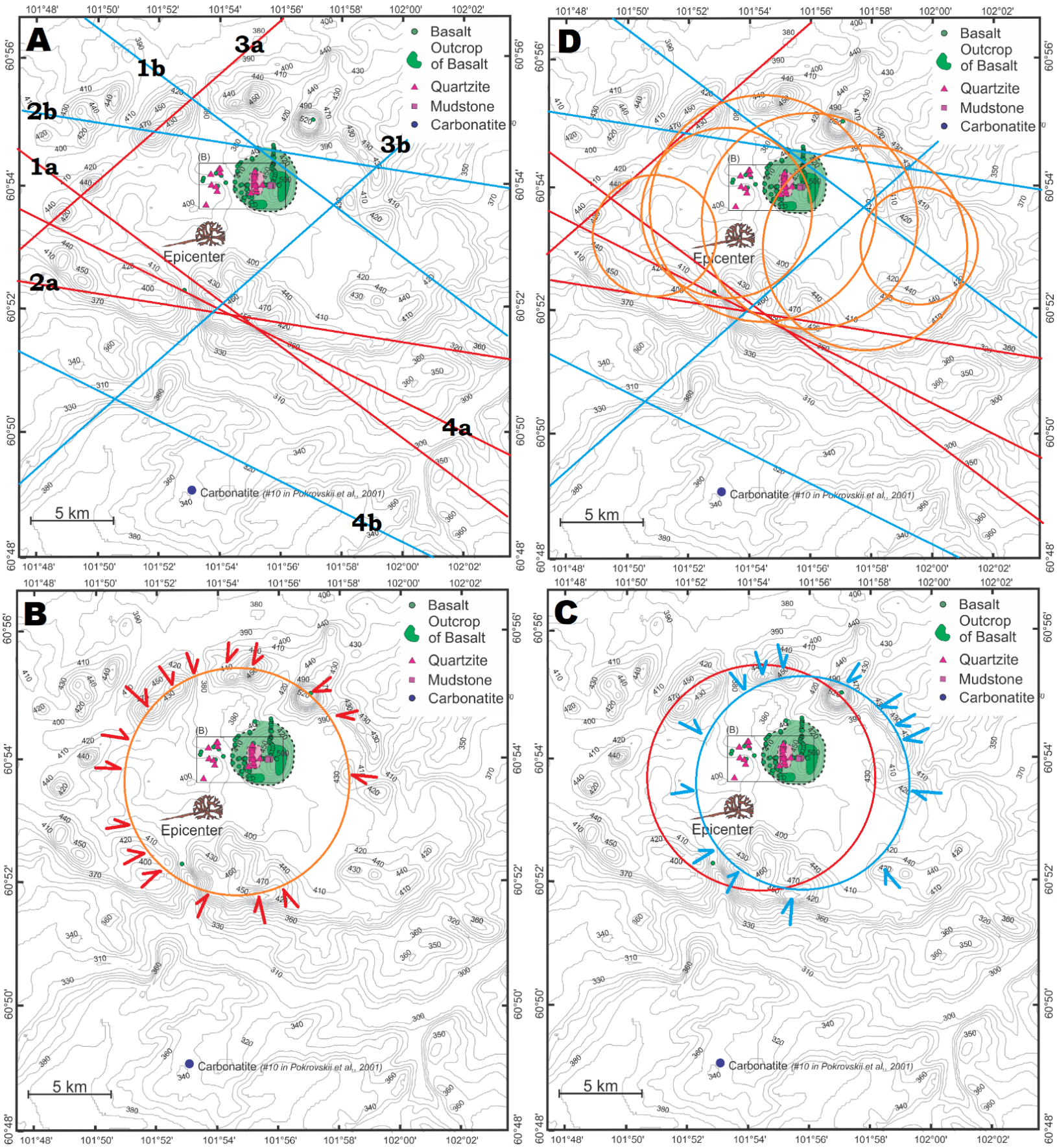

Figure 13.16: Terrane map of Tunguska, Siberia, with no crater forming an impact being recognized, but many ghost craters. (Image credit; modified from Vannuchi et al 2015, their Figure 1A.)

Acknowledgements

Special thanks to Maarten ‘t Hart who created the overlays for Google Earth Moon and Venus for me using cylindrical projection maps of the GRAIL and wrote the program that creates the KML files of cratering centers. He made all of this possible.

References

Bannister, R.A. and Hansen, V.L. 2010, Geologic map of the Artemis Chasma quadrangle (V-48), Venus: U.S. Geological Survey Scientific Investigations Map 3099.

Chiba, T. 2017. Topographic maps of the moon. Freely rotatable red relief maps of the moon globe. Asia Air Survey, Geospatial Information Authority of Japan. https://www.gsi.go.jp/chirijoho/chirijoho41026.html, accessed 12/20/2019.

Giere, R., W. Wimmenauer, H. Müller-Sigmund, R. Wirth, G.R. Lumpkin, and K.L. Smith. 2015. Lightning-induced shock lamellae in Quartz. *American Mineralogist* 100(7):1645-1648.

Giuranna, M., T.L. Roush, T. Duxbury, R.C. Hogan, A. Gaminale, and V. Formisano. 2010. Compositional interpretation of PFS/Mex and TES/MGS Thermal Infrared Spectra of Phobos, *EPSC Abstracts* 5, European Planetary Space Conference 2010-211.

Hryanina, L.P., 1999. The bouquet of the meteorite craters in the epicenter of Tunguska Impact 1908 year. *Lunar and Planetary Science XXX*, Houston, Lunar Planetary Institute.

Hurford, T. A., E. Asphaug, J. N. Spitale, D. Hemingway, A. R. Rhoden, W. G. Henning, B. G. Bills, S. A. Kattenhorn, and M. Walker. 2016. Tidal disruption of Phobos as the cause of surface fractures. *Journal of Geophysical Research, Planets*. 121:1054–1065.

Hyodo, R., H. Genda, S. Charnoz, and P. Rosenblatt. 2017a. On the impact origin of Phobos and Deimos. I. Thermodynamic and physical aspects. The Astrophysical Journal 845:125 (8pp).

Hyodo, R., P. Rosenblatt, H. Genda, and S, Charnoz. 2017b. On the Impact origin of Phobos and Deimos. II. True polar wander and disk evolution. *The Astrophysical Journal* 851:122 (9pp).

JAKA/NHK. 2009. KAGUYA taking "Rupes Altai" by HDTV. https://www.youtube.com/watch?v=dJA-U6ICXeY&index=203&list=PLDA9C6AA8E11F7E56, accessed 4/1/2020.

Kvasnytsya, V., R. Wirth, L. Dobrzhinetskaya, J. Matzel, B. Jacobsen, I. Hutcheon, R. Tappero, and M. Kovalyukh. 2013, New evidence of meteorite origin of the Tunguska cosmic body. *Planetary, Space Science* 84:131–140.

Murry, J.B., and J.C. Iliffe. 2011. Morphological and geographical evidence for the origin of Phobos' grooves from HRSC *Mars Express* images. *Geological Society, London, Special Publications* 356:21-41.

NASA. 2013. *Phobos: Facts and Figures*, NASA, October 19, 2013. https://web.archive.org/web/20131019162634/http://solarsystem.nasa.gov/planets/profile.cfm?Object=Mar_Phobos&Display=Facts, accessed 7/22/2020.

Nayak, M. and E. Asphaug. 2016. Sesquinary catenae on the Martian satellite Phobos from reaccretion of escaping ejecta. *Nature Communications* 7.12591.

Peter H. Schultz & David A. Crawford. 2016. Origin and implications of non-radial Imbrium sculpture on the moon *Nature* 535:391–394.

Pignatale, F.C., S. Charnoz, P. Rosenblatt, R. Hyodo, T. Nakamura, and H. Genda. 2018. On the Impact origin of Phobos and Diemos. III. Resulting composition form different impactors. *The Astrophysical Journal* 853:116 (12pp).

Ronnet, T., P. Vernazza, O. Mousis, B. Brugger, P. Beck, B. Devouard, O. Witasse, and F. Cipriani. 2016. Reconciling the orbital and physical properties of the Martian Moons. *The Astrophysical Journal* 828:109 (7pp).

Soter, S. and A. Harris. 1977. Are striations on Phobos evidence for tidal stress? *Nature* 268, 421–422.

Syal, M. B., J. Rovny, J.M. Owen, and P.L. Millar. 2016. Excavating Stickney crater at Phobos, *Geophysical Research Letters* 43:10,595–10,601.

Vannucchi, P., J.P. Morgan, D.D. Lunga, C. Andronicos, and W.J. Morgan. 2015. Direct evidence of ancient shock metamorphism in the site of the 1908 Tunguska event, *Earth and Planetary Science Letters* 409:168-174.

Wilson, L. and J.W. Head. 2015. Groove formation on Phobos: Testing the Stickney ejecta emplacement model for a subset of the groove population. *Planetary and Space Science* 105:25-42.